# Обзор ArXiv/astro-ph, 22 октября -10 ноября 2021

От Сильченко О.К.

# ArXiv: 2110.13165

# From giant clumps to clouds - II. The emergence of thick disc kinematics from the conditions of star formation in high redshift gas rich galaxies

Floor van Donkelaar[1,2]★, Oscar Agertz[1] and Florent Renaud[1]
[1] *Lund Observatory, Department of Astronomy and Theoretical Physics, Box 43, SE-221 00 Lund, Sweden*
[2]*Center for Theoretical Astrophysics and Cosmology, Institute for Computational Science, University of Zurich, Winterthurerstrasse 190, CH-8057 Zürich, Switzerland*

Accepted XXX. Received YYY; in original form ZZZ

**ABSTRACT**

High redshift disc galaxies are more gas rich, clumpier, and more turbulent than local Universe galaxies. This early era of galaxy formation imprints the distribution and kinematics of the stars that we observe today, but it is not yet well established how. In this work, we use simulations of isolated Milky Way-mass disc galaxies to study how kinematic properties of stars change when varying the gas fraction. This allows us to quantify the roles played by internal processes, e.g. gas turbulence and gravitational scattering off massive gas clumps, in establishing the observed stellar velocity dispersions and orbital eccentricities. We find that models with gas fractions > 20 per cent feature a turbulent and clumpy interstellar medium (ISM), leading to zero-age stellar velocity dispersions $\sim 20 - 30$ km s$^{-1}$ and high mean orbital eccentricities. Low eccentricities cannot arise from these physical conditions. For gas fractions below 20 per cent, the ISM becomes less turbulent, with stellar velocity dispersions $< 10$ km s$^{-1}$, and nearly circular orbits for young stars. The turbulence present in gas-rich high redshift galaxies hence acts as a 'barrier' against the formation of thin discs. We compare our findings to the Milky Way's age-velocity dispersion relation and argue that velocity dispersions imprinted already at star formation by the ISM contribute significantly at all times. Finally, we show that observed orbital eccentricities in the Milky Way's thick and thin discs can be explained entirely as imprints by the star-forming ISM, rather than by mergers or secular processes.

**Key words:** galaxies: evolution – galaxies: structure – Galaxy: disc – methods: numerical

# Постановка задачи

2017; de Jong et al. 2019; Bundy et al. 2015; Bryant et al. 2015). At higher redshift, large galaxy surveys provide insight on the kinematic state of gas and stars in young, intensively star-forming galaxies (see review by Glazebrook 2013). Yet, how high redshift galaxies evolve into the well ordered spirals we observe in the local Universe is a central problem in astrophysics (e.g. Renaud et al. 2021b).

# Индивидуальная динамическая модель Млечного Пути

We achieve high resolution in high density regions using adaptive mesh refinement. A cell is split if its baryonic mass (gas and stars) exceeds 4014 $M_\odot$. In addition, a cell is allowed to refine if it contains more than 8 dark matter particles. This allows the local force softening to closely match the local mean inter-particle separation, which suppresses discreteness effects (e.g. Romeo et al. 2008). The maximum refinement level is set to allow for a mean physical resolution of $\sim 9$ pc in dense gas.

The adopted star formation and feedback physics is presented in Agertz et al. (2013, see also Agertz et al. 2015, 2020) Briefly, star formation is treated as a Poisson process, sampled using star particles of 1000 $M_\odot$, occurring on a cell-by-cell basis according to the star formation law:

$$\dot{\rho}_\star = \epsilon_{\rm ff} \frac{\rho_{\rm g}}{t_{\rm ff}} \quad \text{for} \quad \rho > \rho_{\rm SF}. \tag{1}$$

Here $\dot{\rho}_\star$ is the star formation rate (SFR) density, $\rho_{\rm g}$ the gas den-

$\varepsilon = 10\%$

$\rho = 100$ Cm^-3

SF

The initial stellar and gaseous components follow exponential surface density profiles with scale lengths $r_{\rm d} = 3.4$ kpc and scale heights $z_{\rm d} = 0.1 r_{\rm d}$. The gas disc is initialised at a temperature of $T = 10^4$ K. The total disc mass is $4.5 \times 10^{10}$ $M_\odot$, with the fraction of mass in the gas disc varying between simulations. This allows us to isolate the effect of the gas fraction, which changes the nature of gravitational instability and ISM turbulence on the resulting stellar kinematics (see Renaud et al. 2021a, hereafter Paper I). This approach and the numerical recipe is the same as in Paper I, but we use a different, larger set of initial conditions. The gas fraction is defined as

$$f_{\rm gas} = \frac{M_{\rm gas}}{M_\star + M_{\rm gas}}, \tag{2}$$

where $M_\star$ and $M_{\rm gas}$ is the total stellar and gas mass in the disc

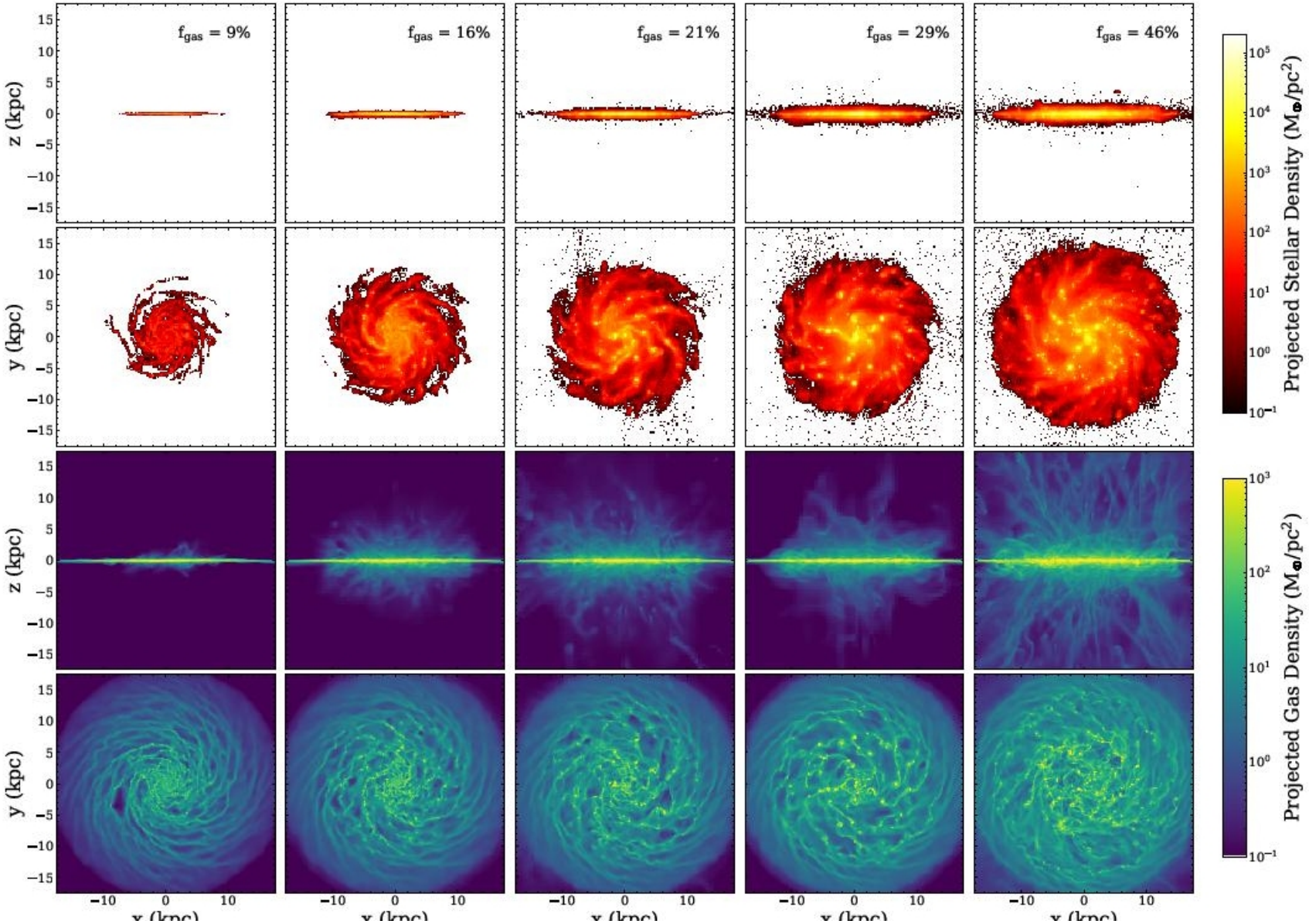


f(gas)_0=10%

f(gas)_0=70%

# Пять моделей

**Table 1.** Properties of the different simulations, all measured at 300 Myr unless otherwise indicated. Simulation names are indicated in column 1. Column 2: gas fraction at 300 Myr; Column 3: star formation rates with the error margins representing the spread in values between 250 and 300 Myr; Column 4: mean velocity dispersion, ±1 standard deviation, of stars younger than 10 Myr; Column 5: approximate redshifts in comparison to Milky Way-like galaxies found by van Dokkum et al. (2013); Column 6: approximate redshifts to allow for birth dispersion to explain the Milky Way's age-velocity dispersion relation (see Section 3.2.1); Column 7: mean eccentricities of stars, ±1 standard deviation.

| Name | $f_{gas}$ (at 300 Myr) per cent | SFR $[M_\odot\ yr^{-1}]$ | $\sigma_{z,birth}$ $[km\ s^{-1}]$ | Redshift (SFR matching) | Redshift (AVR matching) | Eccentricity |
|---|---|---|---|---|---|---|
| fg10 | 9 | 1 ± 0.25 | 5.2 ± 0.4 | 0.0 - 0.2 | 0.0 - 0.2 | 0.10 ± 0.06 |
| fg15 | 16 | 5 ± 0.8 | 8.6 ± 1.8 | 0.5 - 1.7 | 0.1 - 0.4 | 0.33 ± 0.11 |
| fg20 | 21 | 15 ± 2 | 17.9 ± 3.5 | 1.4 - 2.6 | 0.4 - 0.8 | 0.49 ± 0.16 |
| fg30 | 29 | 25 ± 5 | 27.3 ± 3.8 | 1.8 - 2.6 | 0.8 - 2 | 0.53 ± 0.21 |
| fg45 | 46 | 50 ± 10 | 25.8 ± 4.3 | 1.8 - 2.6 | 0.8 - 2 | 0.47 ± 0.22 |

Res ult

Res ult

# Зависимость результатов от доли газа в массе диска

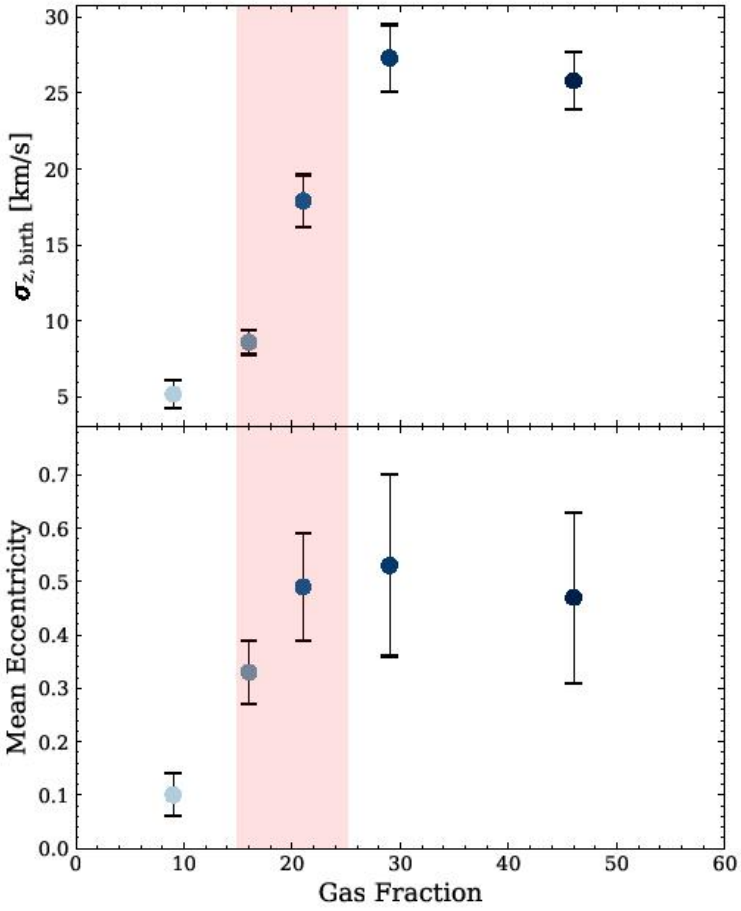


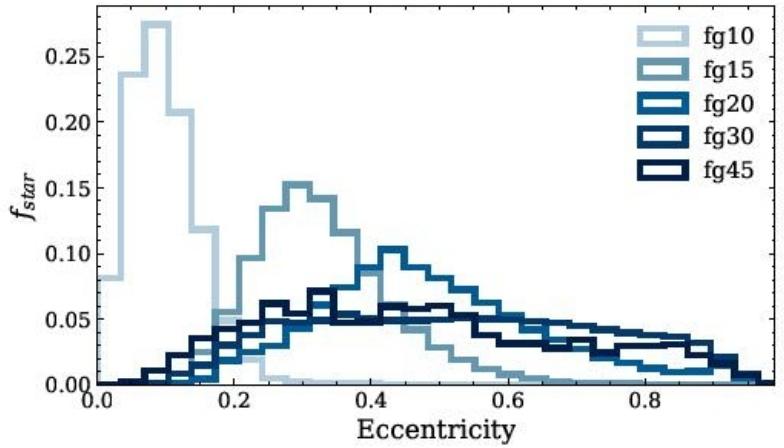


**Figure 3.** The full eccentricity distributions for the different simulations, all stars are included.

# Сравнение с эволюцией AVR в диске Млечного Пути (окрестности Солнца 7-9 кпк)

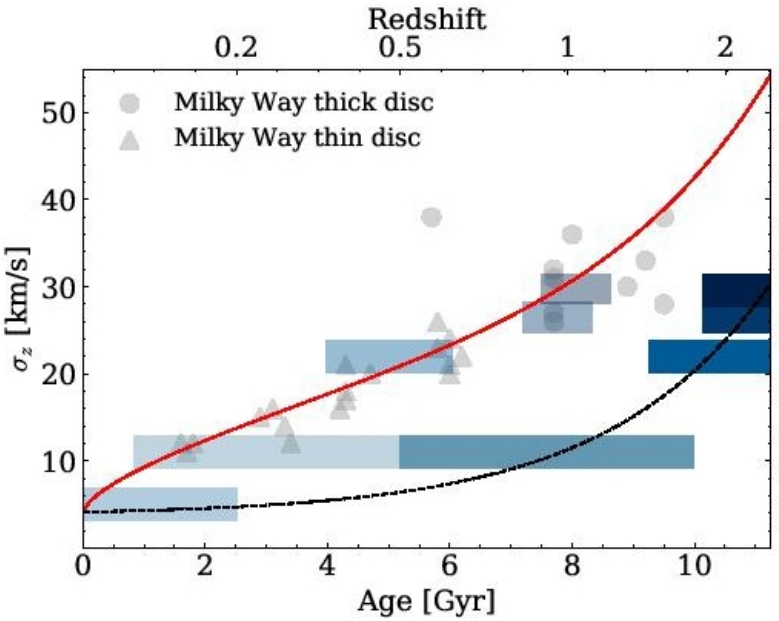


**Figure 4.** The Milky Way's AVR for the thin and thick disc (gray symbols, Mackereth et al. 2019), together with birth velocity dispersions from the simulations, where the associated cosmic epochs are chosen to match the Milky Way data (semi-transparent boxes). The non-transparent boxes show the simulated data at epochs obtained by matching SFRs to observations of Milky Way progenitors, see main text for details. The black dashed line is an exponential fit to this data, and by adding secular heating to this relation, an AVR is obtained (red line) that jointly matches the Milky Way's thick and thin discs.

If we instead retain the originally assigned cosmic epochs to the simulations, secular heating via gravitational scattering of stars off GMCs and massive clumps, spiral arms, and bars occurring over many billions of years, must contribute to the AVR (see review by Sellwood 2014). Aumer & Binney (2017) used $N$-body simulations of galactic discs to study secular heating, and demonstrated that their simulated AVRs are well fitted by a relation that combines secular and birth velocity dispersions, of the form

$$\sigma(t) = \sigma_0 \left( \frac{\text{age}}{10\ \text{Gyr}} \right)^{\beta} + \sigma_{z,\text{birth}}(t)[\text{km/s}]. \quad (3)$$

Here $\sigma_0$ scales the secular heating term, $t$ is the age of the stars, the power law index $\beta$ describes the efficiency of vertical heating, and $\sigma_{z,\text{birth}}(t)$ is the birth velocity dispersion of stars. The last term is often assumed to be a constant, e.g. $6\,\text{km}\,\text{s}^{-1}$ (Aumer et al. 2016b). However, our results show that this underestimates the contribution of birth velocity dispersions in the Milky Way's more gas rich past.

The red line in Figure 4 shows the total heating using Equation 3 with $\sigma_0 = 22.2\,\text{km}\,\text{s}^{-1}$, $\beta = 0.65$ (compatible with the results from Aumer et al. 2016b) and $\sigma_{z,\text{birth}}(t)$ obtained from our simulations (dashed line). This AVR provides a good match to the Milky Way data, and jointly reproduces the thick and thin disc data points in the Solar neighbourhood. This joint match cannot be achieved without the contribution from a varying $\sigma_{z,\text{birth}}(t)$ in Eq. 3.

# Лучший тест происхождения толстого диска: некруговые орбиты

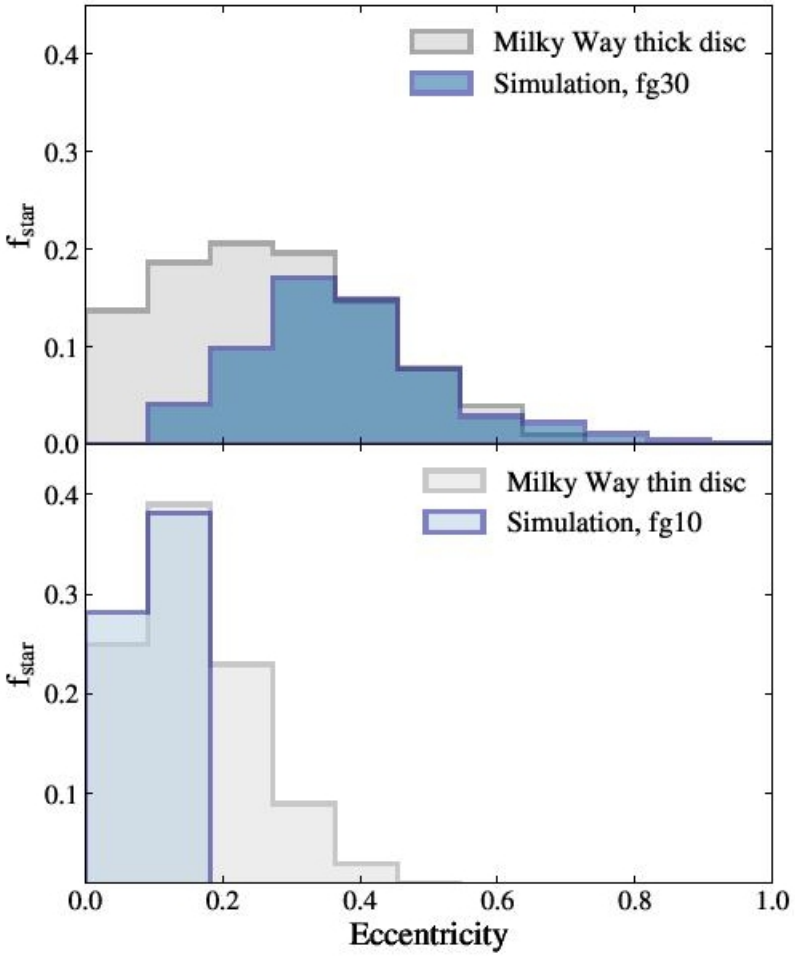


As seen in Figure 5, the tail of high eccentricities ($\gtrsim 0.4$) in the thick disc distribution is well matched by stars that have formed in the gas rich disc. This means that cosmological processes, such as mergers, are not necessary to explain such high eccentricities. We re-emphasize that this is not due to slow secular processes (e.g. radial migration, Sales et al. 2009), but an imprint of the turbulent and clumpy ISM. However, to explain the existence of eccentricities $\lesssim 0.1 - 0.2$, lower gas fractions are required. This may indicate that the thick disc's gas fraction decreased rapidly in the early Universe, while retaining a high [$\alpha$/Fe]. The redshifts obtained from our SFR matching are compatible with this notion, as $f_{\rm gas}$ decreases from 50 to 20 per cent in less than a Gyr at $z \sim 1.5$ (see Table 1). Alternatively,

# ArXiv: 2111.04864

## The two formation pathways of S0 galaxies

Simon Deeley[1]*, Michael J. Drinkwater[1], Sarah M. Sweet[1,2,3], Kenji Bekki[4], Warrick J. Couch[2], Duncan A. Forbes[2], Arianna Dolfi[2]

[1]*School of Mathematics and Physics, University of Queensland, Brisbane, Queensland 4072, Australia*
[2]*Centre for Astrophysics & Supercomputing, Swinburne University, Hawthorn, VIC 3122, Australia*
[3]*ARC Centre of Excellence for All Sky Astrophysics in 3 Dimensions (ASTRO 3D)*
[4]*International Centre for Radio Astronomy Research, The University of Western Australia, 35 Stirling Highway, Crawley, Western Australia, 6009, Australia*

Accepted XXX. Received YYY; in original form ZZZ

**ABSTRACT**

Despite their ubiquity throughout the Universe, the formation of S0 galaxies remains uncertain. Recent observations have revealed that S0 galaxies make up a diverse population which is difficult to explain with a single formation pathway, suggesting that the picture of how these galaxies form is more complicated than originally envisioned. Here we take advantage of the latest hydrodynamical cosmological simulations and follow up these studies with an investigation into the formation histories of S0s in IllustrisTNG. We first classify IllustrisTNG galaxies in a way which is fully consistent with the observations, and reproduce the observed photometric and environmental distributions seen for the S0 population. We then trace the formation histories of S0 galaxies back through time, identifying two main distinct pathways; those which experienced gas stripping via group infalls (37 percent of S0s) or significant merger events (57 percent). We find that those forming via mergers feature a transient star-forming ring, whose present-day occurrence rate matches observations. We find that these formation pathways together can reproduce the range in rotational support in observed S0s, concluding that there are two main formation pathways for S0 galaxies.

# IllustrisTNG100 – это наше ВСЕ


**Figure 1.** Comparison of mock rgb SDSS images generated from IllustrisTNG (top row) with real SDSS images of equivalent SAMI galaxies (bottom row). The mock SDSS images were used to classify the galaxies.

**Позволяет глазомерную классификацию типа**

# Расхождение с наблюдаемыми корреляциями как-то не волнуют..

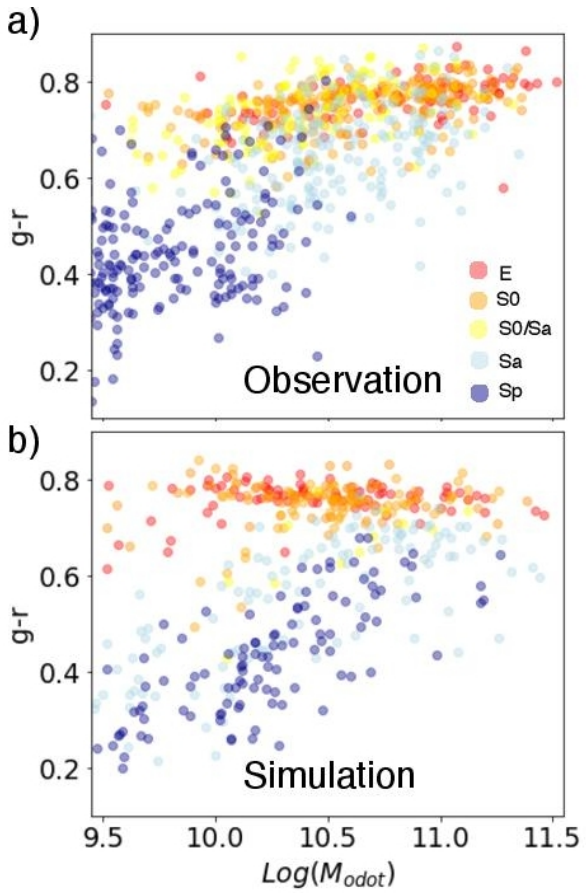


**Figure 2.** Comparison of our IllustrisTNG sample with the SAMI survey i colour-mass plane. Both samples are coloured by their visual classificat

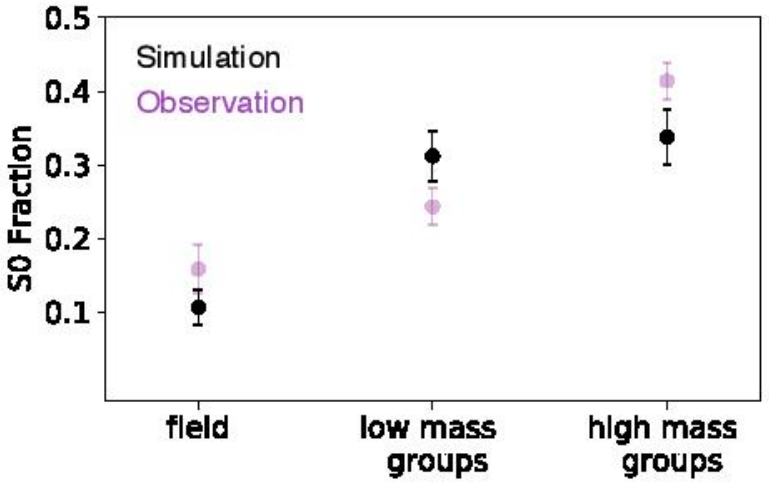


**Figure 3.** Fraction of galaxies classed as S0 as a function of their host environment for both our IllustrisTNG-100 simulation sample (black) and the SAMI observational sample (purple). Field, low mass groups and high mass groups correspond to host halos with a total mass less than $10^{12}$ $M_{\odot}$, between $10^{12}$ and $10^{13}$ $M_{\odot}$, and above $10^{13}$ $M_{\odot}$ respectively. The relative fraction of S0s in our simulation sample closely follow those of observations across different environments. The cluster fields in the SAMI survey are left out due to the lack of these environments within the simulated volume.

# Кинематические карты с достаточным разрешением

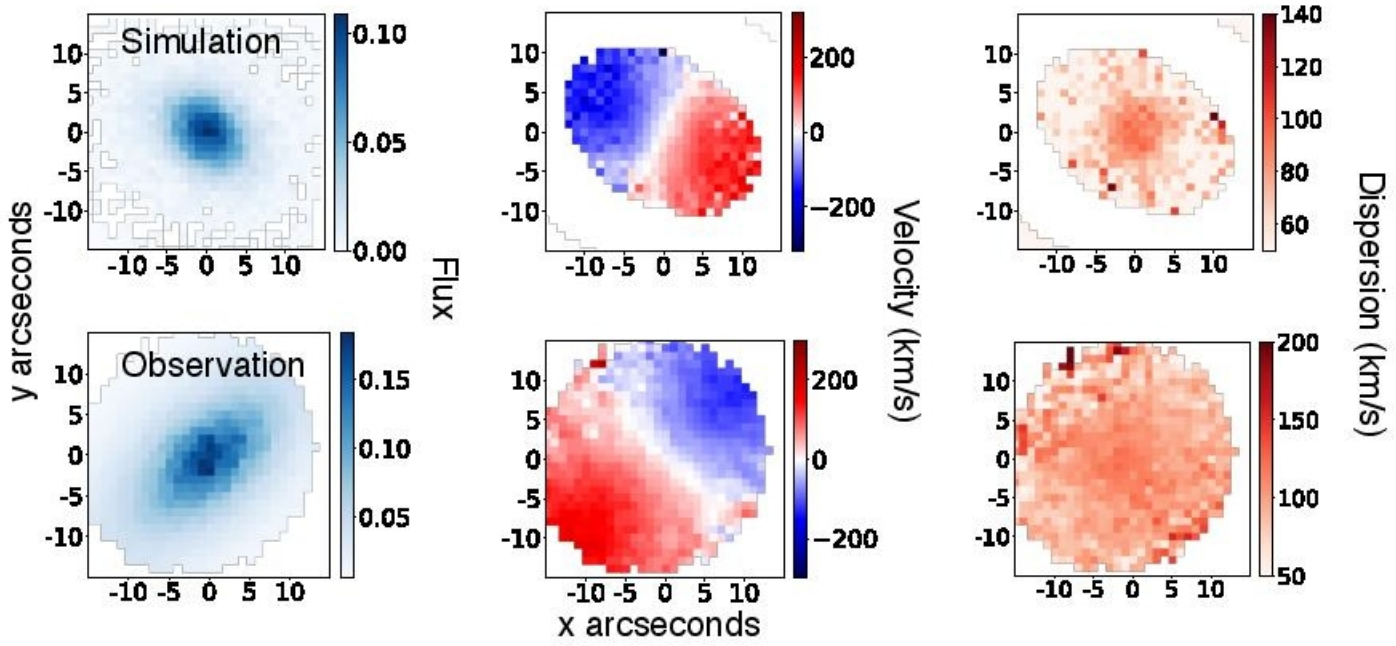


**Figure 4.** An example of the stellar kinematic maps derived for the IllustrisTNG-100 galaxies (top row) compared to those of an example galaxy from SAMI (bottom row). The left column shows the flux, the middle column shows the line-of-sight velocity map, and the right-most column displays the velocity dispersion map.

**Хотя в наблюдениях - диски, а в симуляциях - балджи**

# Результат: два основных сценария для 127 модельных S0

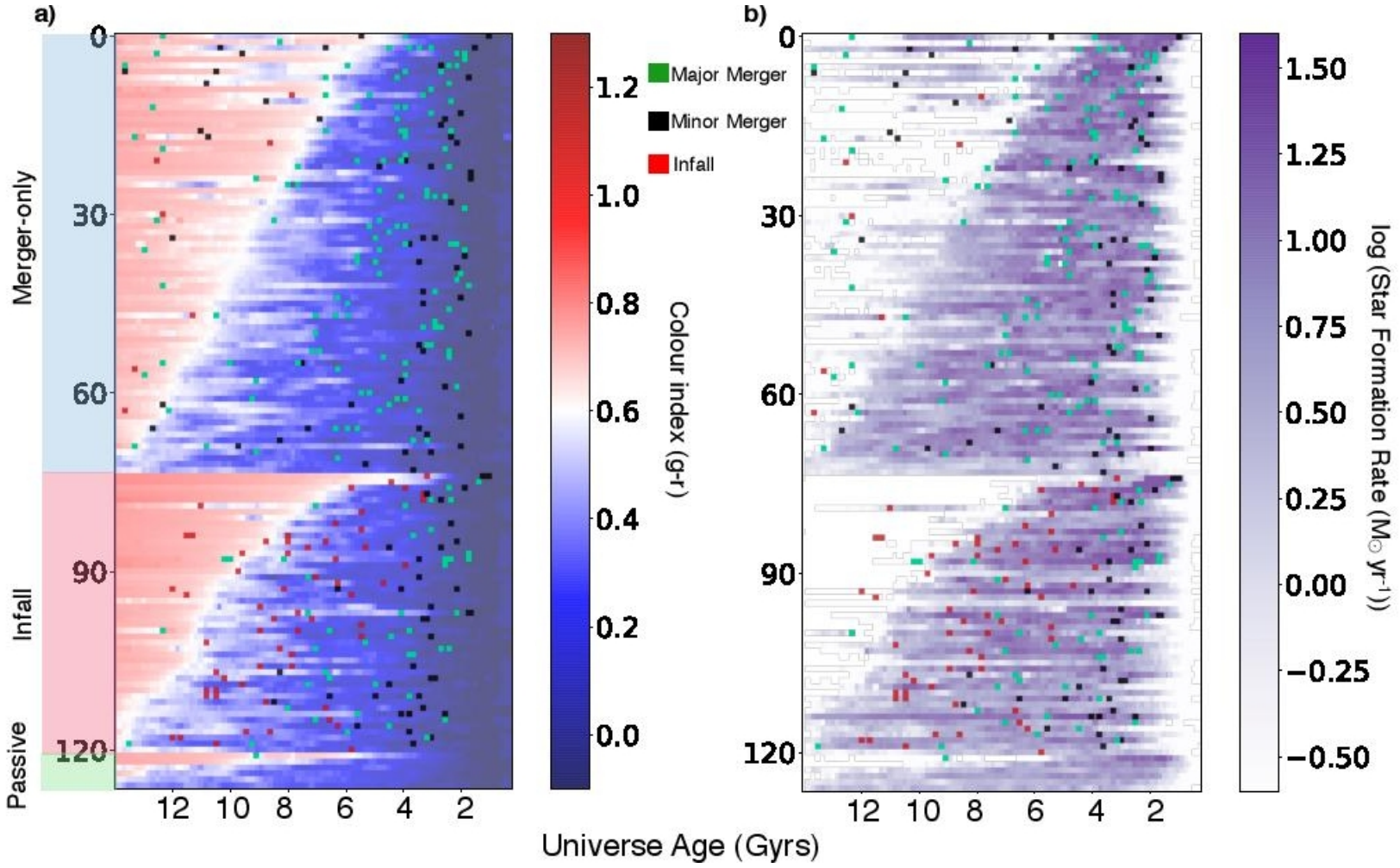

# А это эволюция газа в них же

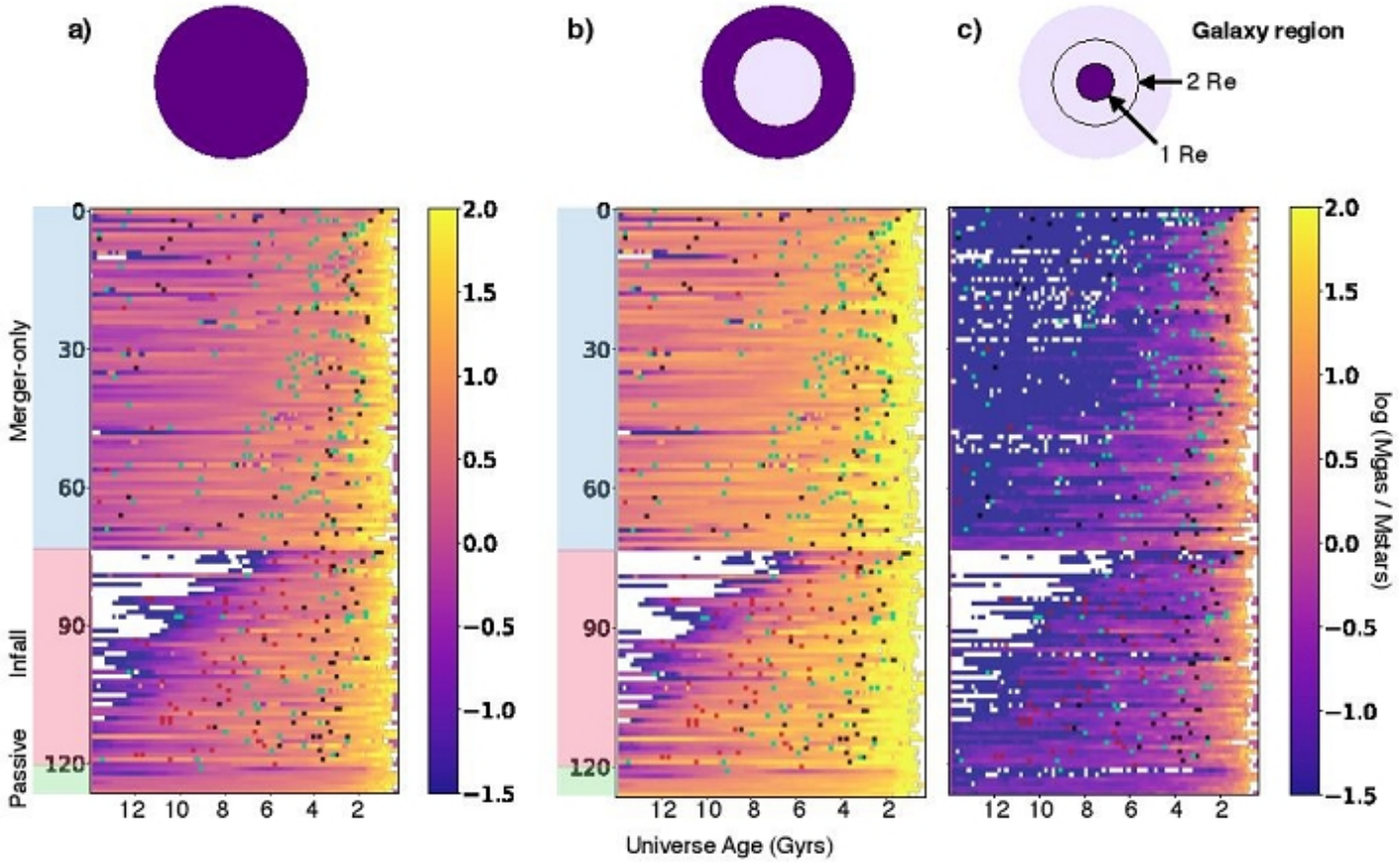


**Figure 6.** History plots of the gas contents of S0 galaxies, within the galaxy regions highlighted by the dark purple regions in the circles along the top. a) shows the total gas mass normalised by the stellar mass, highlighting the stripping occurring for the passive and infall pathways. b) and c) show the gas content within 1 Re and beyond 2 Re respectively, illustrating that while the merger group retain a large amount of gas, this gas is located in the outskirts while the central regions have become largely devoid of gas.

# Пример ободранной S0

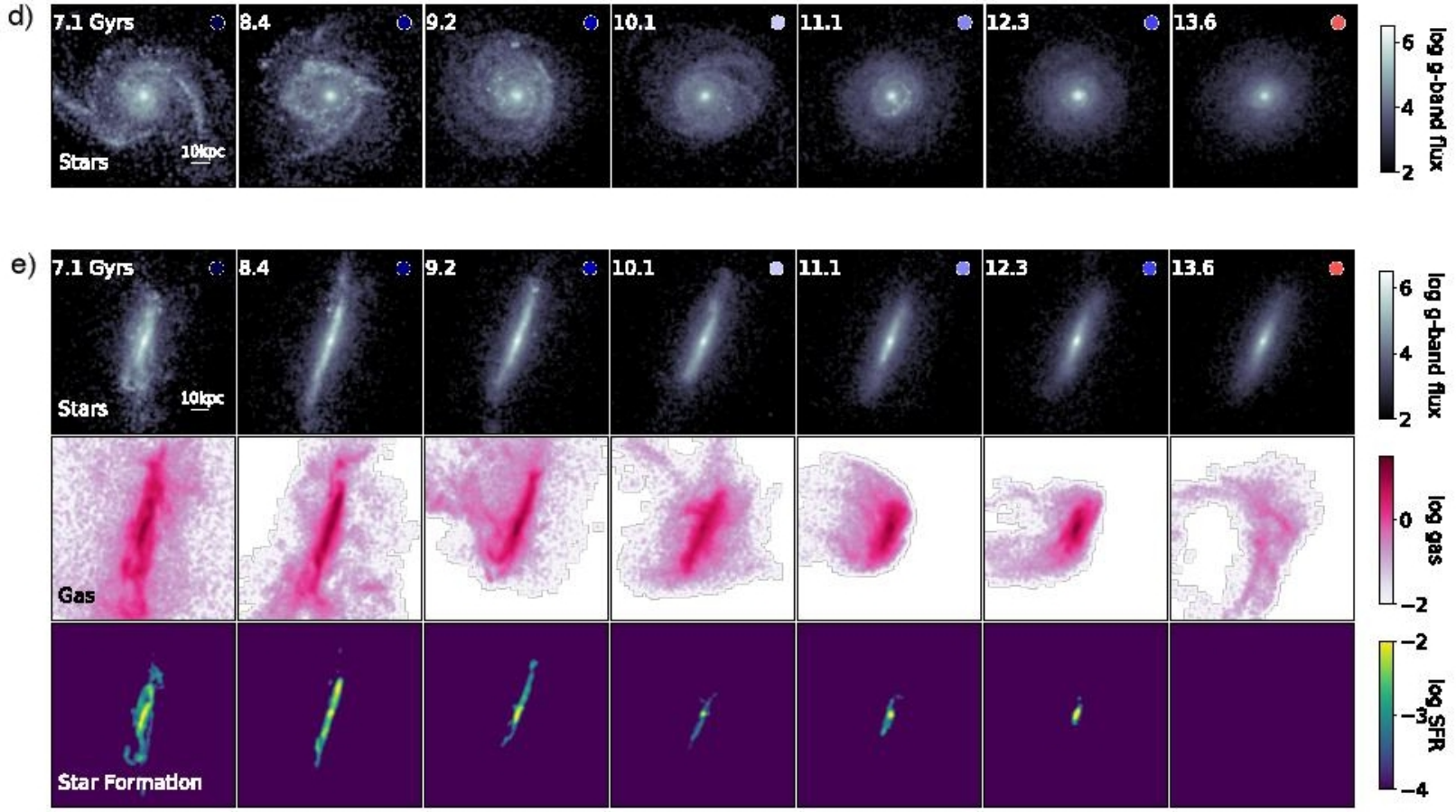


**Figure 8.** An example of an initially blue, gas-rich galaxy falling through the centre of a galaxy group and having its gas stripped out. The purple region in a),

# Пример S0, построенной мержингом

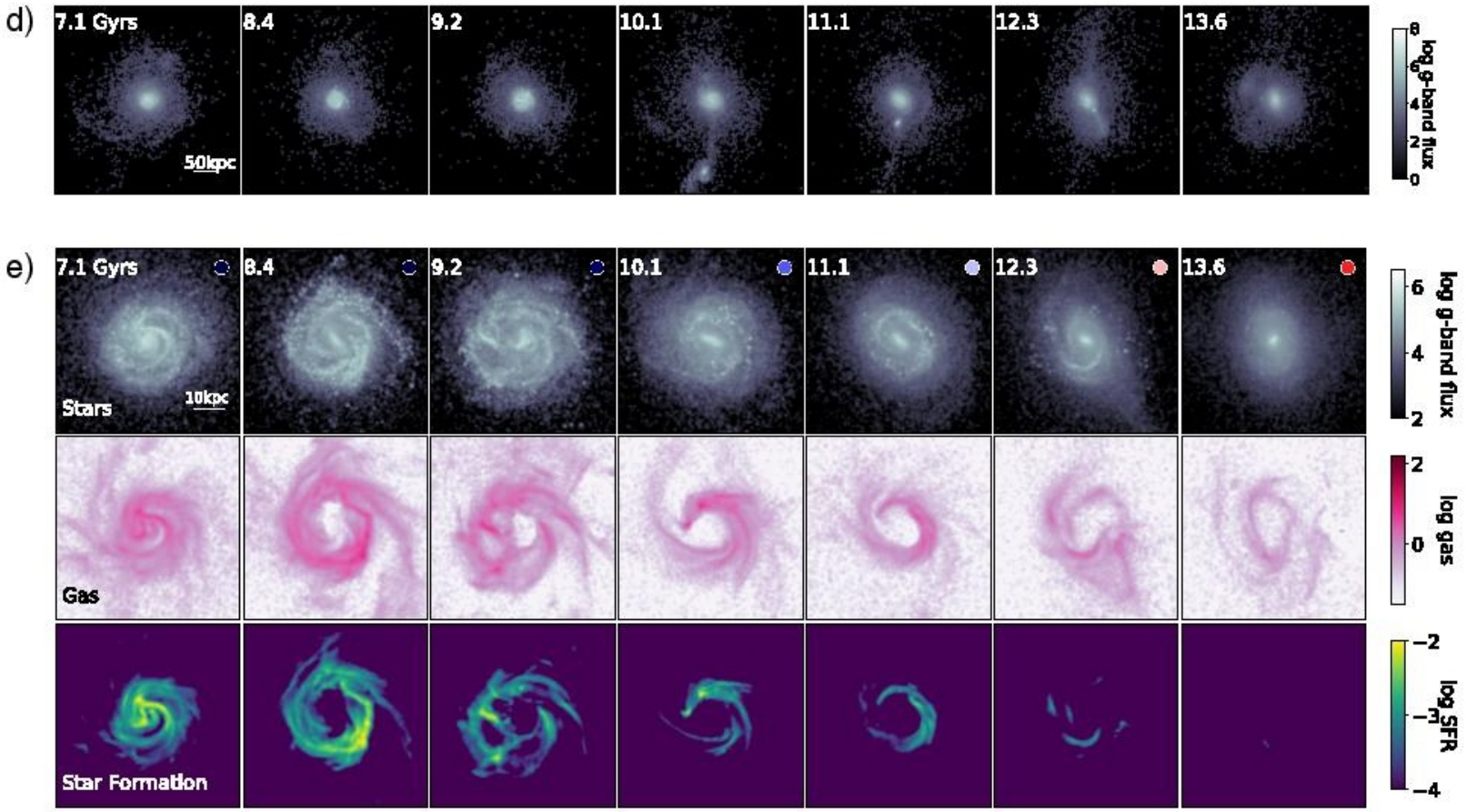


**Figure 9.** An example of a spiral galaxy transforming to an S0 after multiple merger events. a) and b) are the same as in Figure 8, while the points in c) are

# Пример S0, которая сама по себе S0

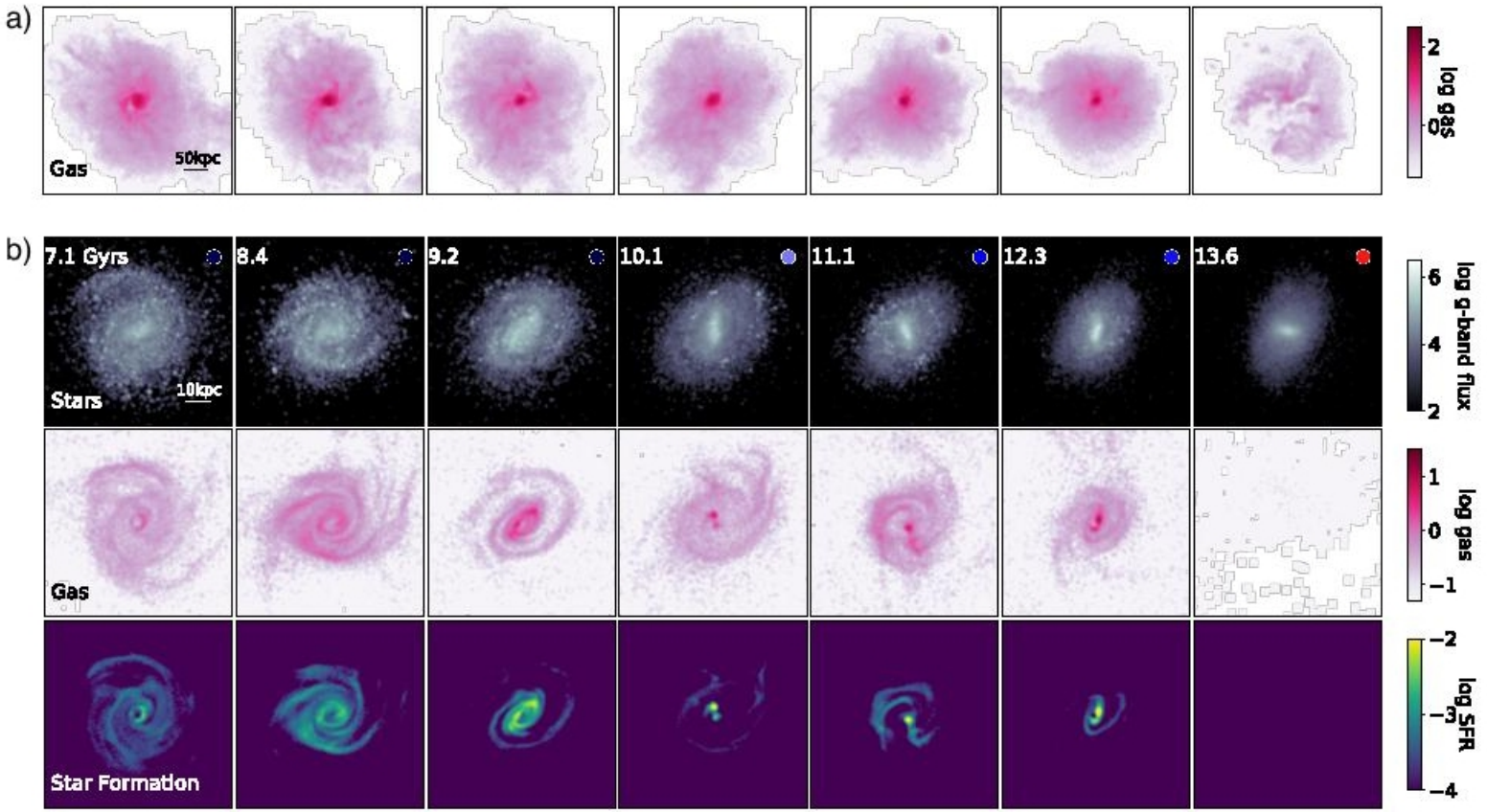


**Figure 11.** Typical example of the evolution of an S0 which experiences no significant events. a) shows a larger-scale view, highlighting the depletion of the extended gas halo. b) shows the evolution in the stellar luminosity, gas and star formation rate as in Figure 8, showing the outside-in quenching of star formation and the gradual loss of the spiral arms.

# Отдельная песня про кольца SF

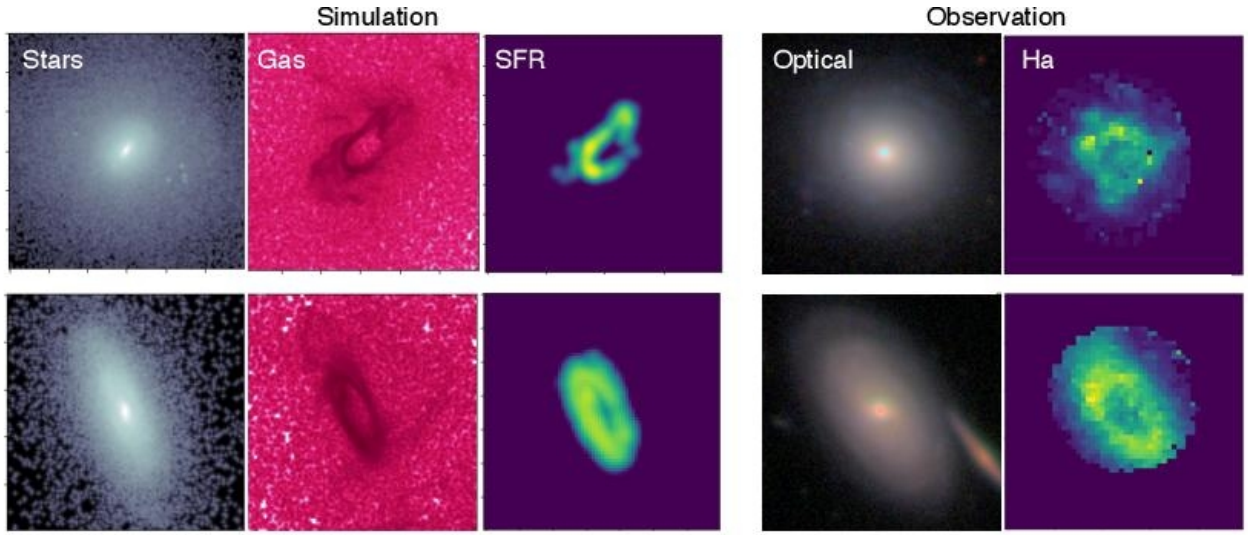


**Figure 10.** Comparison of the morphology of the star forming rings with H$\alpha$ observations taken from SAMI. From left to right, the plots show distributions of stars, gas and star formation of two example illustrisTNG S0s, and the right column shows examples of the observed H$\alpha$ flux in two SAMI galaxies. The first row illustrates a clumpy, irregular ring and the second illustrates a smooth, coherent ring, showing that both morphology types can be reproduced by the merger pathway.

Visual inspection of the SFR distributions of all S0s reveals that nearly all S0s in the merger group (and many in the infall group which experience a merger prior to the infall event) go through a phase where a clear SFR ring is present, appearing soon after the merger event. The average lifetime of the rings is very brief, typically around 1-2 billion years, meaning that despite their ubiquity, we would expect to observe only a small number of S0s with SFR rings in today's observations. Indeed, in SAMI we identify 10 clear rings out of 146 galaxies in the GAMA region, an occurrence rate of 7 percent. For comparison, the number of rings observed in snapshot 91 (at a redshift of 0.1) is 6.5 percent, remarkably close to the occurrence rate in SAMI.

# Сравнение кинематики с SAMI

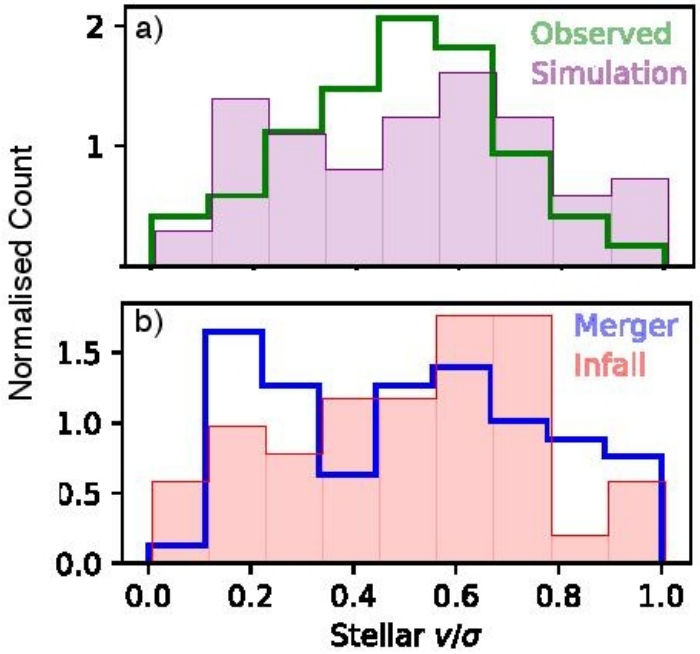


**Figure 13.** Distributions of the S0 stellar $v/\sigma$, using line-of-sight projections. a) compares the observed SAMI S0 sample (green) with the illustrisTNG sample (purple), showing that the range of rotational support in the simulation S0s is similar to observations. b) shows the $v/\sigma$ distribution for IllustrisTNG S0s in the merger-only group (blue) and the infall group (red).

To assess the degree of rotational support, following Deeley et al. (2020) we employed the widely-used parameter $v/\sigma$, where v is the observed line-of-sight velocity and $\sigma$ is the velocity dispersion. We calculate $v/\sigma$ using the following equation:

$$\left(\frac{v}{\sigma}\right)^2 = \frac{\sum_{i=0}^{N_{spx}} F_i V_i^2}{\sum_{i=0}^{N_{spx}} F_i \sigma_i^2}, \quad (1)$$

where the sum is over all spaxels within a de-projected radius of 1.5 $R_e$ and $F_i$ is the flux of spaxel $i$. Values of $v/\sigma$ approaching 1 indicate a rotationally supported structure, while values towards zero indicate a pressure-supported structure. The de-projected radius of each spaxel corresponds to the major axis of the ellipse on which it is located, which was determined using the $r$-band-derived axis ratio and position angle.

# Два сценария для происхождения S0 работают в разном окружении

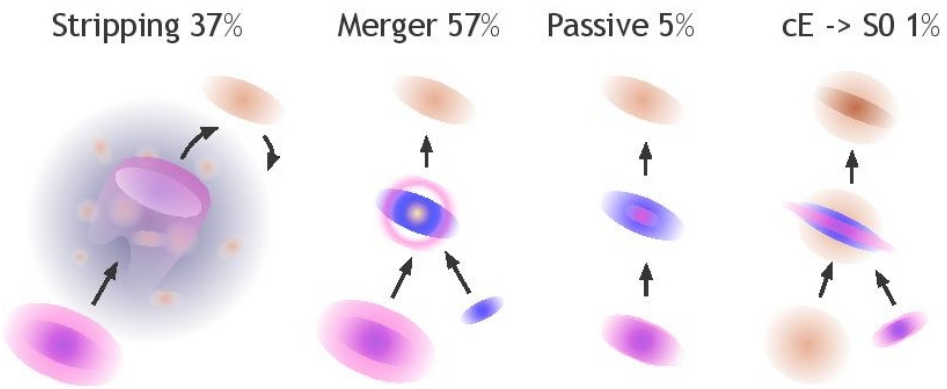


**Figure 16.** The overall picture of S0 formation presented in this work. Blue - young stellar populations, orange - older stellar populations, pink - gas, purple - intra-cluster medium.

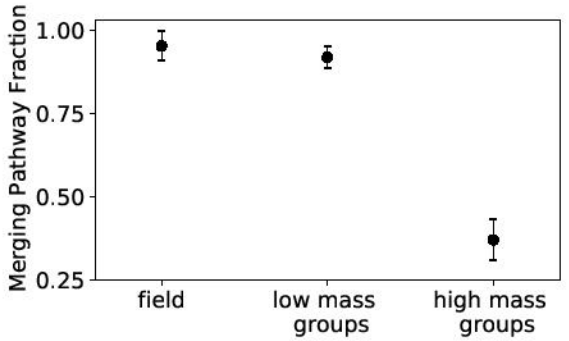


**Figure 12.** The relative occurrence of the merger pathway in different environments. S0s forming via the merger pathway dominate in low density environments while those forming via stripping dominate the high-density environments. Even though this is initially unsurprising since higher density environments are required for the infall pathway to occur, this interestingly suggests that there is very little pre-processing in these environments, i.e. very few galaxies within these groups entered the group after already transforming into an S0. However it should be noted that pre-processing may be more common in higher-density cluster environments.